Practical Investigation into the Diffusion Bonding of 316L Stainless Steel with Boron Carbide for Radiation Shielding in Nuclear Thermal Propulsion Applications

By

Calvin Chandler

Mechanical and Aerospace Engineering Department

The Ohio State University

April 15th, 2022

Advisor:

Dr. John M. Horack

Abstract

Diffusion Bonding is a solid-state welding process in which two or more materials are bonded together into one seamless structure under high temperature, vacuum, and pressure conditions without requiring any external fixations. This process allows for the creation of complex structures impregnated with substances that possess qualities comparable to their base components, while at the same time, producing negligible adverse effects on the final product's material properties. For example, design limitations in radiation shielding for spacecraft commonly require the structures to possess low weight and exceptional material properties when produced. This investigation evaluated the interdiffusion regions in and around the bond of 316L stainless steel with boron carbide while supporting and validating the creation of the first physically bonded sample between the two materials. This research assists and grows the current work put into Diffusion Bonding as an additive manufacturing technique, strengthening its use in aerospace, nuclear, and manufacturing applications.

Acknowledgements

I would like to thank Dr. John Horack and Noah Gula from the Department of Mechanical and Aerospace Engineering at the Ohio State University for their integral assistance in the field of nuclear thermal propulsion. In addition, I would like to thank Dr. Antonio Ramirez, Dr. Elvin Beach, and Wayne Papageorge from the Department of Material Science and Engineering at the Ohio State University for their assistance in microscopy analysis and material prepping. I would also like to thank Dr. Zhijun Jia from CompRex, LLC. for his instrumental expertise in the field of Diffusion Bonding. Finally, I would like to thank Timothy DeFranco for his support and feedback during this investigation in addition to his parallel research project, the *Computational Investigation into the Diffusion Bonding of 316L Stainless Steel and Boron Carbide for Radiation Shielding in Nuclear Thermal Propulsion Application*.

List of Figures

List of Abbreviations

Table of Contents

I. Introduction

I.I. The Basics of Nuclear Thermal Propulsion

Future space missions, especially those wishing to reach deep space targets, will require propulsion systems with performance far exceeding modern rocket engines to reach their destinations in a reasonable amount of time. Rocket engine systems today typically employ chemical or solid-based fuel systems with specific impulses ranging from 350-540 and 200-260 seconds respectively [1]. One solution proposed to increase rocket efficiency is the Nuclear Thermal Propulsion (NTP) system based on the designs produced during the Nuclear Engineering for Rocket Vehicle Applications (NERVA) program conducted by the United States government in the 1960s and 70s. The NERVA rocket design is shown in Fig. 1 below.

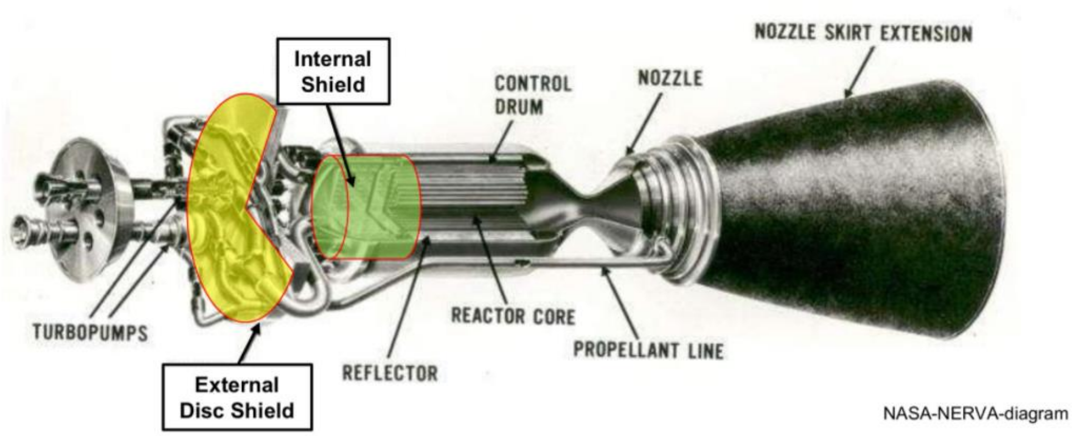

Figure 1: NERVA Rocket Engine Design [2]

The NERVA rocket design saw specific impulses as high as 901 seconds with a thrust as high as 166.1696 kN [3]. To reach such high specific impulse, NTP rocket engines emit thermal energy through nuclear fission processes in the reactor core. This thermal energy is then absorbed by the fuel, typically liquid hydrogen, as it is passed through the core and converted into kinetic energy. Finally, the fuel is expanded through the engine nozzle to reach incredibly high exhaust velocities near 9000 m/s [3].

I.II. Radiation Shielding

Another major factor to consider with NTP is the radiation generated from the activity of the reactor core in the engine. The radiation generated during engine operation is not only dangerous for the crew during manned missions, but also to any critical instrumentation contained within the spacecraft. To prevent substantial damage or even death, care much be taken when designing the shielding to create a well-designed, thought out, and constructed apparatus. There must be a careful balance in the shielding components' cost and materials (typically with a multilayer configuration shown in Fig. 2 below). Effective radiation shielding requires "a considerable thickness of high-density material" that is also resistant to high neutron flux levels and temperatures present in a Nuclear Rocket Engine (NRE) [4].

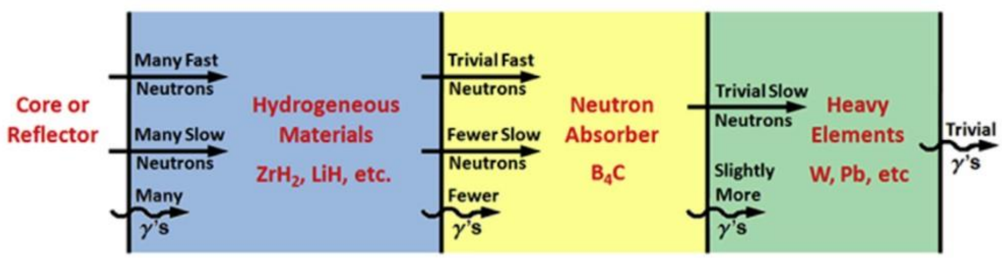

Figure 2: Typical Multilayer Shield Configuration [4]

There are several different kinds of radiation that can be emitted by a nuclear reactor, including alpha particles, beta particles, positrons, neutrons, x-rays, and gamma rays. However, in NTP applications, the most important types of radiation to consider are neutrons and gamma rays [4].

There are two classifications of neutrons: fast neutrons, and thermal or slow neutrons. Fast neutrons have relatively high energy, greater than 1 MeV, while slow neutrons have relatively low energy, less than 1 eV. Since fast neutrons have high energies, they typically have much lower cross sections, or probability of interacting with matter while passing through it. Therefore, using a material, typically hydrogen-bearing materials, capable of slowing the fast neutrons down to thermal energy levels is ideal [4]. Once the fast neutron energies have been reduced to a trivial level, the slow neutrons can be absorbed by a neutron absorber, typically boron carbide (B4C) [4]. However, after absorbing a thermal neutron, boron will emit an alpha particle and gamma ray [5]. Gamma rays are very harmful to humans because they have the energy to pass through the human body and force out electrons from atoms in sensitive tissue and organs. The emitted gamma rays from boron, as a result of the absorbed a neutron, have an energy of 0.48 MeV [5]. For gamma radiation with energies of less than 1.5 MeV, shielding is dominated by photoelectric absorption and Compton scattering [6]. Compton scattering varies with Z, the atomic number of a material, and the photoelectrical effect varies as Z^4 [7]. Therefore, heavy elements with high atomic numbers, such as tungsten and lead, are ideal for dealing with gamma rays as another layer of shielding after B4C.

I.III. Diffusion Bonding

In recent years, research and development into solid-state welding techniques have seen significant growth in aerospace, nuclear, and advanced manufacturing application. Traditional joining and additive manufacturing techniques such as Selective Laser Sintering or Brazing have been used to bond dissimilar materials into complex parts. However, these processes can introduce micro-fractures and other imperfections which detrimentally affect the final product. These shortcomings can be overcome by applying solid-state welding techniques, such as Diffusion Bonding (DB), on a layer-by-layer basis to create composite structures. The typical DB process uses high pressure and high temperature environments, like an isotropic hot press furnace, to molecularly bond materials together in a homogenous manner without sacrificing the desirable properties of the base materials. Fig. 3 below outlines the fundamental principles of DB.

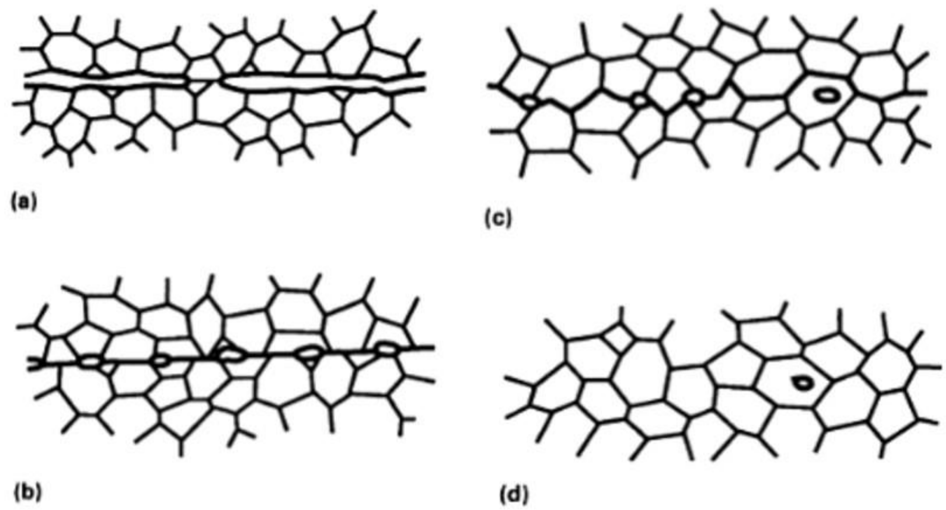

Figure 3: The DB Process: a) Initial Connection; b) First stage of DB; c) Second Stage of DB; d) Final Stage of DB [8]

In Fig. 3 (a), the initial contact of the material asperities at room temperature takes place before the DB process begins. This step is followed by Fig. 3 (b), the first stage of deformation that causes an interfacial boundary layer due to material creep. The second stage of the DB process is represented in Fig. 3 (c) where grain boundary migration and pore elimination occur between the materials. Figure. 3 (d) illustrates the final stage of the process where the pore elimination and volume diffusion of the atoms fills the voids and creates a seamless product at the diffusion location [8]. The resulting product leads to the creation of complex structures whose properties are remarkably like those of the base material while lessening the overall structural and thermal damage to the final product.

Once the DB process is completed, the bond quality is analyzed by a microstructure analysis using optical microscopy. Using a powerful microscope to enhance the image of the bonding layer 400 or 500 times, judgement can be made about the overall quality of the bond between the two materials. Figure 4 (a) below represents a bond of poor quality while Fig. 4 (b) represents a bond of high quality. Two distinct qualities are present in the right image that are representative of most high-quality bonds: the faded bonding line shows that sufficient diffusion between the materials has occurred, and the smaller grain structure compared to the poor bond indicates that the resulting material will retain its material properties [9]. An increase in the grain size of a material decreases the number of grain boundaries per unit are in a material. As a result, an applied force has a greater chance of fracturing the material at the grain boundary than in a sample with a small grain size [10].

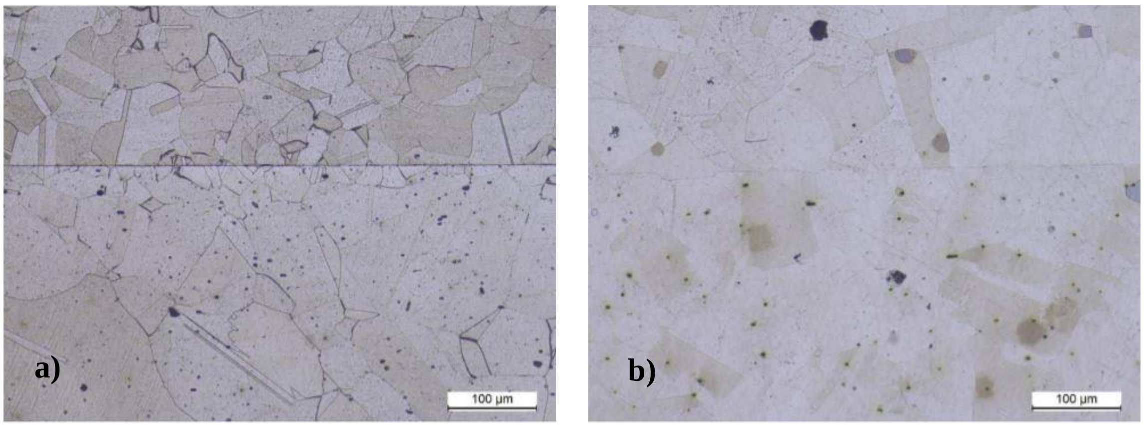

Figure 4: Microscopy of a) Poor DB and b) Good DB [9]

In the past, DB has typically been used to create metal-metal bonds. Previous research suggests that the three main parameters during the process of DB are temperature, time, and pressure, with temperature being the most important parameter due to its effects on mass transport kinetics and atomic mobility through the boundary layer interface [9]. In metal-metal bonds, the temperature required to obtain sufficient joint strength is typically 50%-80% of the base material's melting point [11]. However, in metal-ceramic bonds, "bonding temperatures of up to 90% of the metal's melting point have been reported" to achieve sufficient bonding between the materials [11].

While there is research into DB between metals and ceramics, there is little to no current literature about the application of DB applied to 316L stainless steel (ss) and B4C. Therefore, the primary goal this research project is to produce of a physical sample and a material analysis to highlight the effects introduced into the structure by the joining process. The results obtained by this research could reduce overall costs, energy, and time to produce high-quality metallurgicalcontaining components and expand the current body of academic literature. In addition, the newly generated compound materials could broaden the application of DB to various aerospace and NTP applications, and many manufacturing fields. The work done on this project will serve to provide a fundamental understanding of the material properties needed to utilize 316L ss efficiently and effectively in nuclear, aerospace, and other fields of interest.

I.IV. Uses and Properties of 316L Stainless Steel and Boron Carbide

316L ss and B4C are both very common materials in the application of nuclear power and radiation protection. 316L ss is valued for its corrosion and radiation resistance while B4C is valued for its neutron absorption properties. However, B4C, like many ceramics, has a low fracture toughness, making it unsuitable for structural applications [12]. However, if B4C was reinforced by 316L ss using DB, the applications of B4C could be broadened.

The material properties of 316L ss and B4C are very important, to assess the feasibility of DB. Relevant material properties of 316L ss and B4C to DB are shown below in Fig. 5 and Fig. 6. Because of the large difference in melting point between 316L ss and B4C (Max. Use Temperature), DB applications can be difficult. However, these materials also have properties that promote bonding with each other and the overall strength of the bond. First, the small amount of Carbon in 316L ss will promote bonding with the carbon in B4C.

Another important characteristic of 316L ss and B4C is their coefficient of thermal expansion (CTE). The CTE of for 316L ss is $18.0x10^{-6}\ K^{-1}$ [14], and B4C's CTE is $6.3x10^{-6}\ K^{-1}$ [15]. While these differences are not extreme in magnitude, they become more pronounced at higher temperatures, and given the very high temperature requirement of this bond, the CTE can have a drastic impact on the materials. During the cooling process after the materials have been joined, they begin to shrink according to their CTE, exerting forces on the bonding layer. A large difference between the CTE of two materials can cause significant and irreparable damage to the sample.

PHYSICAL PROPERTIES

Melting Point	Density	Specific Gravity	Modulus of Elasticity in Tension
2540-2630° F 1390-1440° C	.29 lb/in³ 8.027 g/cm³	8.03	29 X 10^6 psi 200 Gpa

MECHANICAL PROPERTIES

Alloy	Temper	Tensile Strength Minimum (psi)	Yield Strength Minimum 0.2% offset (psi)	% Elongation in 2" Minimum	Notes
316L	Annealed	70,000	25,000	40 %	-

All values specified are approximate minimums unless otherwise specified. Values are derived from the applicable AMS and ASTM specifications.

CHEMICAL PROPERTIES

Alloy	C	Mn	P	S	Si	Cr	Ni	Mo	Cu	N	Other
316L	**.03**	2.00	.040	.030	1.00	16.00-18.00	10.00-14.00	2.00-3.00	.75	-	-

All values are maximum values unless otherwise specified. Values are derived from applicable AMS and ASTM specifications.

Figure 5: Material Properties of 316L ss [13]

Thermal		
Max. Use Temperature (in air)	°C	2450
Thermal Shock Resistance	ΔT (°C)	ng
Thermal Conductivity	W/m-K @ R.T.	28
Coefficient of Linear Thermal Expansion, α_l	10^{-6} K^{-1} (~25°C through ±1000°C)	945
Specific Heat, c_p	J kg^{-1} K^{-1} @ R.T.	0.25

Figure 6: Thermal Properties of B4C [12]

Finally, the bonding strength of metal-ceramic bonds tends to increase linearly with the melting point of the metal, as shown in Fig. 7 below. Because the melting point of 316L ss is relatively high at 1390 to 1440 degrees Celsius, there is a higher likelihood that the bond between 316L ss and B4C will be strong.

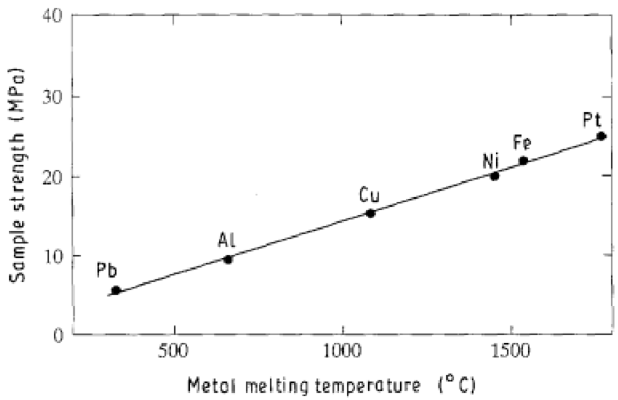

Figure 7: Effect of Metal Melting Temperature on Bond Strength of Metal-Ceramic Joints [11]

II. Methodology

II.I. Diffusion Bonding

A furnace capable of the high conditions required by the DB process with 316L ss and B4C was needed to acquire a workable sample for research. CompRex, LLC. in La Crosse, Wisconsin, was contacted to use an adequate furnace for these conditions. Because of the increased bonding conditions required in metal-ceramic bonds [11], and the overall lack of literature specific to this application, the required bonding conditions were approached with caution. Based on this approach, and on conversations with Dr. Jia from CompRex, LLC. as an expert on the subject, the bonding conditions were determined to be a temperature of 1160 degrees Celsius, and a pressure of 200 psi (1.38 MPa). Additional capabilities on site at CompRex, LLC. allowed the bonding conditions to be altered during the joining process while monitoring characteristics of the bond quality formation. As experts in the field, employees at CompRex, LLC. monitored the compression rates of materials due to the temperature and pressure. However, they determined that there were no required adjustments during the bonding process, so the initial conditions remained throughout the duration of the bond.

After the bonding of the sample was completed, the sample was shipped to the Ohio State University for practical testing. Unfortunately, the substantial difference in the CTE between the two materials caused the sample to be compromised during the cooling process. The thermal contraction of the materials caused a thin layer of B4C still attached to the 316L ss to be ripped from the bigger block of B4C. Figure 8 (a) shows the thin laminate layer of B4C remaining on the 316L ss after thermal contraction, and Fig. 8 (b) shows the remaining block of B4C. Further structural testing of the sample was unable to be performed because the results of the test would not be representative of the true material properties of the created structure. However, since a thin layer of B4C was attached, the sample was still analyzed to determine the bond quality between the two materials.

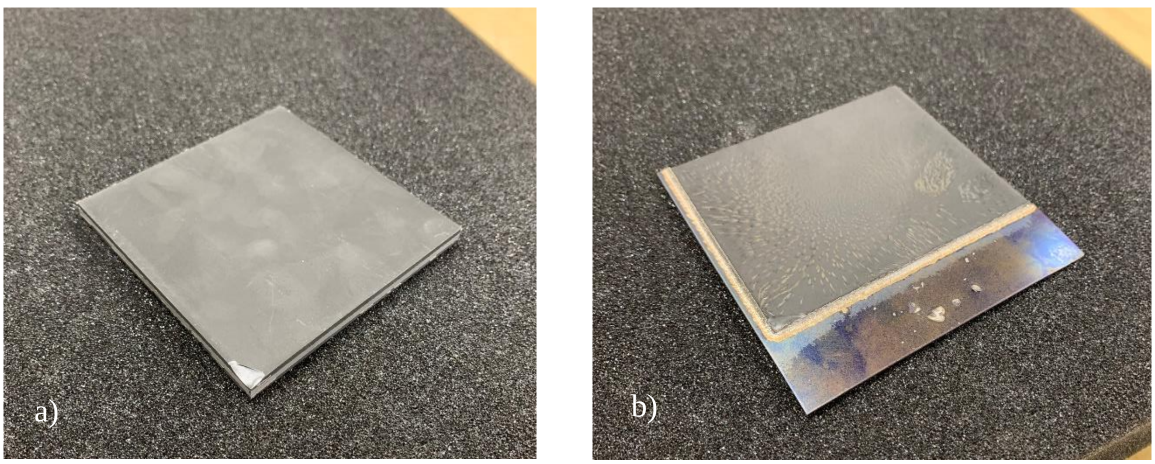

Figure 8: Bonded Sample After Thermal Contraction: a) B4C, b) Remaining Bonded Sample

II.II Material Prepping

Given the toughness of B4C, a diamond wheel cutter, shown below in Fig. 9, was required to cut the sample. A total of three cuts were performed on the workable samples to provide a final sample for bond quality evaluation tests. Figure 10 below shows the result of the first cut performed on the composite sample, and Fig. 11 shows the results of the remaining two cuts to prepare the final sample for analysis. Highlighted in Fig. 10 is a silver smudge. Initially the diamond wheel was not tightly secured to the machine which caused it to cut into the B4C without making a clean cut. This anomaly does not compromise the quality of the bond in the rest of the sample, and therefore did not impact the bond strength and quality of the final sample.

Figure 9: Diamond Wheel Cutter

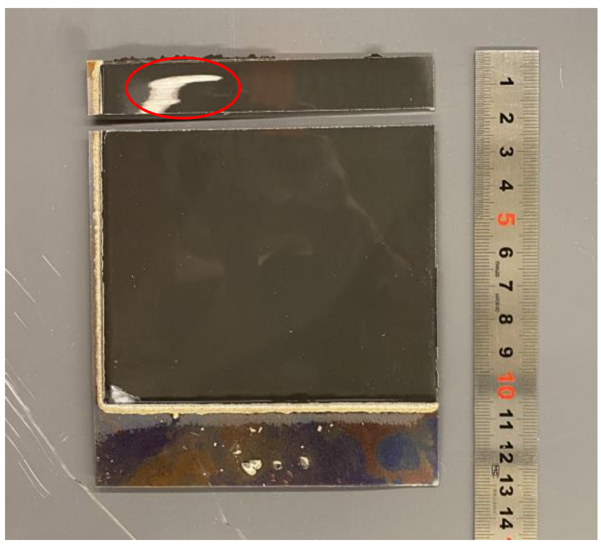
Figure 10: First Cut in the Composite Sample

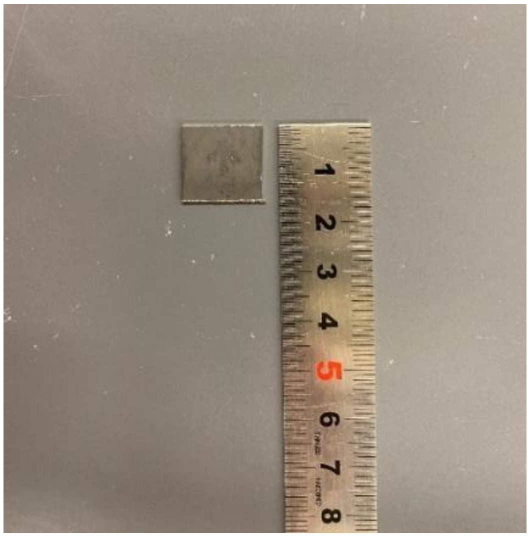

Figure 11: Final Sample

After the cuts were completed, the final sample was place in a cold mount epoxy resin mold. A cold mount was used because a hot mount would have applied too much pressure on the sample. Once the resin set, shown below in Fig. 12, a manual polisher grinder, shown below in Fig. 13, was used to remove the harmful effects of the blade on the material and allow inspection of the bonding layer rather than any influence of the blade. Grit ratings of 320, 400, 600, 800, and 1200 were used in an increasing order to gradually smooth-out the surface of the boundary layer. A final polish was performed with 0.05-micron colloidal silica. Water was continually applied to the surface where the polisher grinder and sample met to keep the surface cooled and to wash away any debris. Additionally, between each grit rating the sample was washed to remove any remaining particulates from the larger grit, and alcohol was used to dry the sample before the sample was inspected with a microscope to determine the quality of the polish. After inspection, the sample was returned to the polisher grinder to continue the polishing process until the image of the sample was satisfactory.

Figure 12: Final Sample in a Cold Mount

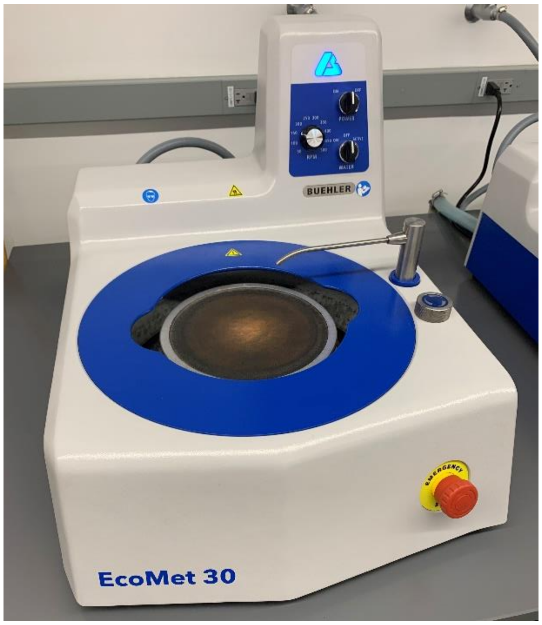

Figure 13: Manual Grinder Polisher

II.III. Optical Microscopy

The final polished sample was imaged using an Olympus DSX510 shown in Fig. 14 below and using an Olympus GX53 shown in Fig. 15 below. The software “DSX Software” was used with the Olympus DSX510, and the software “PAXcam” was used with the Olympus GX53 to control the camera and settings to take images of the sample. The Olympus DSX510 was used to take composite images of the whole sample at 130, 250, and 550 magnifications. Based on these images, three regions were identified for further imaging. The Olympus GX53 was used to take images showing the edge of the sample, a representative image of the bonding line, and an image of an uncommon anomaly near the bonding line, each taken at 100, 200, and 500 magnifications. All microscopy images are shown in Appendix A.

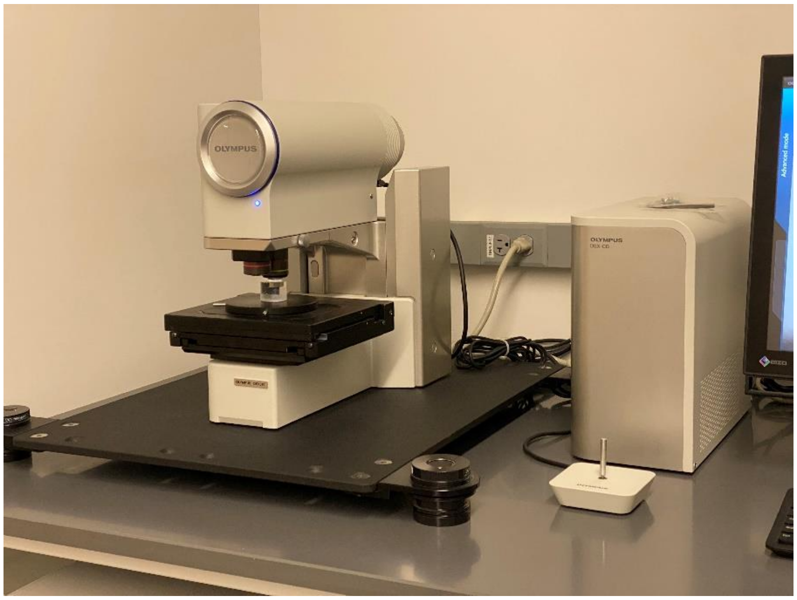

Figure 14: Olympus DSX510 with Sample Mounted

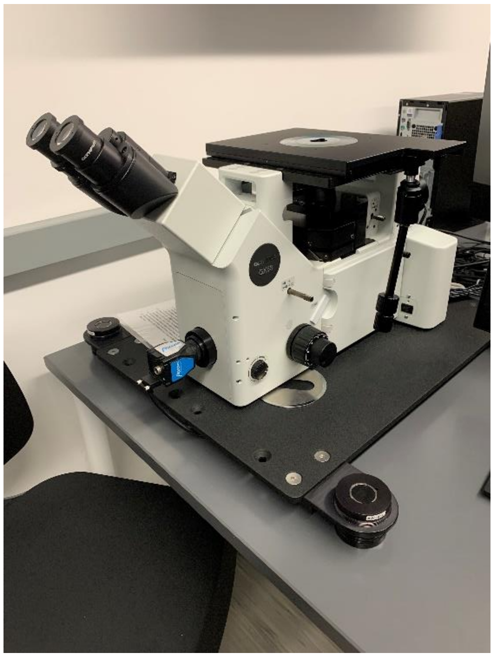

Figure 15: Olympus GX53

III. Discussion and Results

III.I. Visual Indicators of a Strong Bond

Even before a more intense inspection of the bond boundary layer, visual inspection and critical thinking of the sample's characteristics could indicate certain properties about the bond. The most immediately noticeable feature of the sample is the laminate layer of B4C on the 316L ss. While the separation of this laminate layer from the main B4C block is undoubtedly undesirable for any practical application, the fact that the laminate layer exists has positive implications on the bond strength and quality of the sample. B4C is one of the hardest known materials after diamond. The laminate layer of B4C indicates that the bond was strong enough to oppose the shearing force caused by thermal contraction during the cooling process. Another possible indicator of a strong bond lies in the highlighted silver smudge in Fig. 10. If the bond strength was poor, the two materials would have delaminated, and the sample would have been rendered useless.

However, while these features indicate that a strong bond is likely in this application, they are not certain measures of bond strength but rather merely inferences based on known characteristics. Regardless of the implications of these observations, the bond strength and quality may still be poor, and these occurrences may have been coincidence or lucky. To properly access the bond strength and quality of the sample, at least two additional tests need to be performed. First is optical microscopy to assess the bond quality of the sample. Second is a three-point and/or four-point flexural test to assess the bond strength of the sample. However, these physical properties tests are impractical to perform on the sample discussed in this research due to the thermal contract shear. As such, these tests would not be representative of a usable material obtained through DB.

III.II. Optical Microscopy Images

Optical microscopy images were inspected to assess the bond quality of the sample. Several aspects of these images are applicable to understanding the bond quality. First, the boundary line of the sample can be compared to known high-quality bonds. Second, unique features of the sample can be observed, and their implications assessed. Finally, a measurement of the thickness of the 316L ss can be made to understand at least partially what happened during the joining process.

The most important factor of a high-quality bond is the appearance of the boundary line between the two materials. A representative image of the sample's bond quality at 200 times magnification is shown in Fig. 16 below. The red line drawn on the image shows approximately where the boundary line between the two materials was at the start of the joining process. This shows that much of the diffusion between 316L ss and B4C occurred as the B4C diffused into the 316L ss. While it is unusual for so much of only one material to diffuse into another, this was expected in this case due to the hardness and high melting point of B4C. However, the boundary line is not solid as seen in Fig. 4 (a) and is more Fig. 4 (b), indicating that the bond quality in the sample is high.

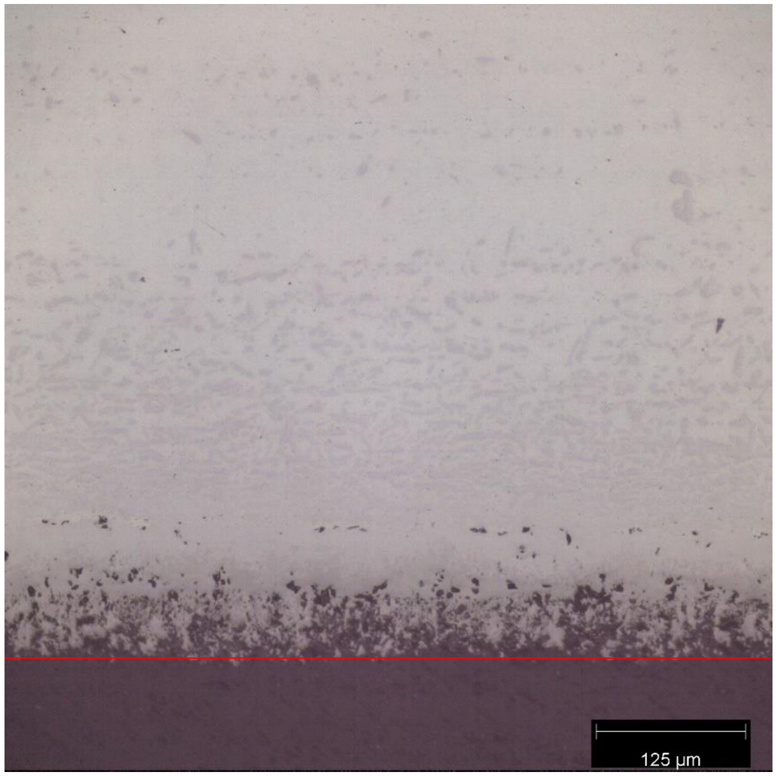

Figure 16: Representative Bond Quality Image at 200 Times Magnification

The optical microscopy images also reveal interesting anomalies in the sample that are not typically present in DB. Fig. 17 below shows an image of the sample at 550 times magnification that was adjusted post-imaging for clarity of significant aspects of the sample. The discolored portion of 316L ss above the nominal diffusion line of B4C and the short lines dispersed throughout the 316L ss are both uncharacteristic of DB results. The specific causes of these anomalies are unknown, but there are some likely possibilities. In addition to the high temperature used during the joining process, high pressure on a material also lowers the melting point of that material. Melting typically does not occur during DB. However, with theses uncharacteristically high temperature and pressure conditions, the 316L ss may have melted, or come close to melting, near the bonding line of the B4C. While melting is not necessarily desirable, the magnitude of diffusion of B4C into 316L ss could be a result of this melting. The high pressure could also contribute to the appearance of the lines in the 316L ss, which may be a result of too much compression in the material.

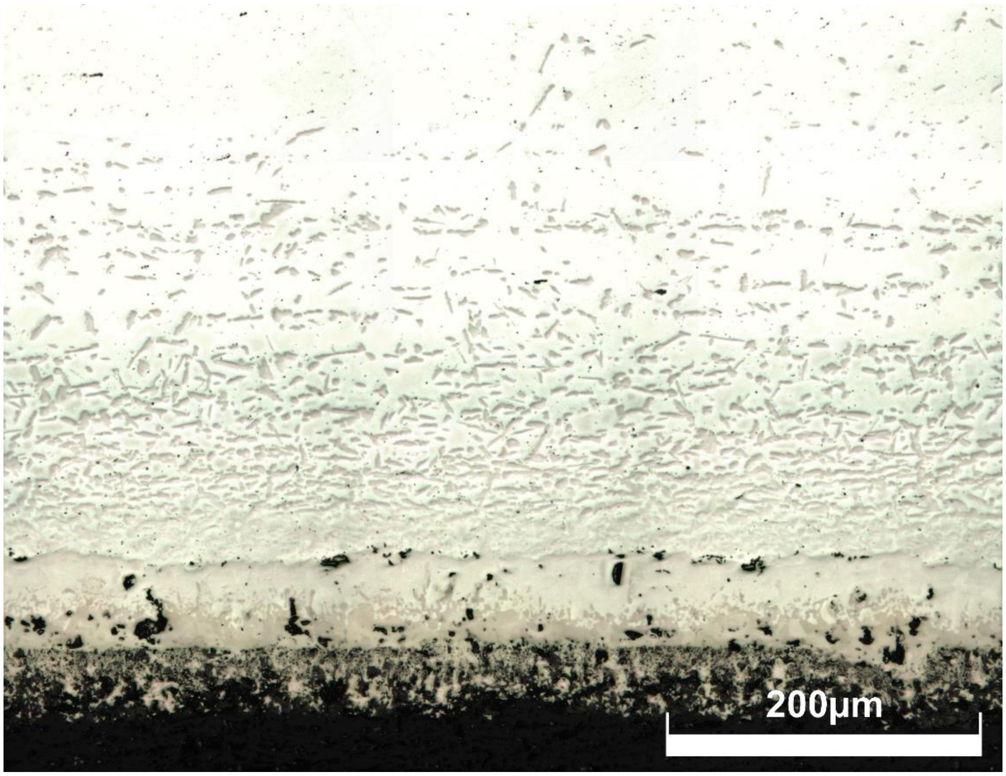

Figure 17: Composite Image Adjusted for Clarity at 550 Times Magnification

While the effects of these irregularities on the material properties of the complex material are unknown, the physical strength of the material was likely compromised. These properties of the material can be tested. However, since the sample in this research is not representative of a usable material, such tests would be impractical, as their results would not be consistent with future bond's material strength. To test these irregularities, a full material that does not shear due to thermal contraction needs to be manufactured.

IV. Conclusion and Future Work

IV.I. Bond Strength and Quality

Based on the acquired optical microscopy images, DB between 316L ss and B4C can result in high-quality bonds. However, the bond strength between the two materials is much less certain. There are some factors, shown in Fig. 8 and Fig. 10, that indicate the bond strength could be excellent, while there are other factors, the irregularities shown in Fig. 16, that indicate the bond strength could be poor. However, the irregularities in Fig. 16 could also mean that the physical strength of the resulting material is poor even if the bond between the two base materials is strong.

More research on the material irregularities and reducing the effect of thermal contraction during the cooling process needs to be performed. A stronger understanding of these irregularities would be fundamental to applications of DB to metal-ceramic joints and the use of the resulting materials in NTP, material science engineering, and construction.

IV.II. Addition of an Interlayer During Diffusion Bonding

One method of reducing the effect of thermal contraction on the bond would be to introduce an interlayer during the DB process. This is one of the next planned steps for this project. Adding another material during the cooling process would introduce a gradient in the CTE between the materials and potentially reduce the thermal contraction forces on the B4C. One of the best materials for this use could be a pure Nickel interlayer. Nickel is a very common material to use as an interlayer in welding applications, and it has certain properties that could make it particularly effective in this application. As shown in Fig. 5, Nickel constitutes a significant percentage of 316L ss. In addition, Nickel's CTE is $14.00x10^{-6}\ K^{-1}$ [16], which is between 316L ss's CTE of $18.0x10^{-6}\ K^{-1}$ [14], and B4C's CTE of $6.3x10^{-6}\ K^{-1}$ [15]. However, typically the addition of an interlayer does not interfere with the bond of the two base materials. In this application, the thickness of Nickel would likely be large enough to the point that the DB process would apply between 316L ss to Nickel and then Nickel to B4C.

While a strong bond between 316L ss and Nickel is likely, the result of a bond between Nickel and B4C would be unknown. However, the melting point of Nickel is 1440 degrees Celsius [16] which is very similar to the melting point of 316L ss, 1390-1440 degrees Celsius [13]. Therefore, the conditions of the high vacuum hot press furnace would need to be nearly identical as in the 316L ss-B4C bond. The Carbon in 316L ss that aided in the bonding with B4C, however, is not present in Nickel. This could lower the quality and strength of a bond between Nickel and B4C.

IV.III. Material Strength Testing

After a representative sample is acquired, material properties testing can take place. The results of these tests, such as the three-point and four-point flexural tests, serve a twofold purpose. First, they will show the properties of the resulting complex material, such as the elastic modulus, flexural stress, flexural strain, and the material’s flexural stress-strain behavior. These properties will indicate the various use-cases of the material. Second, depending on the test used and the failure location in the material, the bond strength can be evaluated.

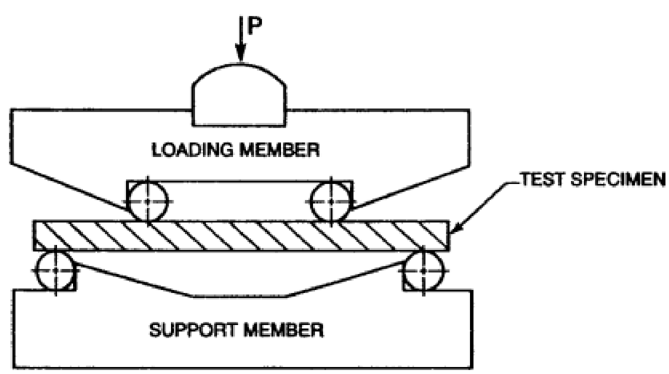

Figure 18: ASTM C1161 Configuration for Four-Point Flexural Test [17]

The four-point flexural test, shown above in Fig. 18, is recommended for this project due to the presence of the ceramic material of B4C in the material. The four-point flexural test is the standard test method for flexural strength of advanced ceramics at ambient temperature as posed by the American Society for Testing and Materials (ASTM) C1161. The four-point flexural test requires a simple set-up and simple geometry easily machinable from the rectangular form of the sample. This test is also ideal for materials involving ceramics because it spreads the maximum stress on the material over a larger area. However, sample preparation is of extreme importance for this test. If there are any cracks in the ceramic material, the property results will be significantly reduced and the results will not be representative of the true material. In addition, the location of the failure in the material relative to the bonding line and potential irregularities in the material, like the irregularities in Fig. 17, will qualify the bond strength.

IV.IV. Radiation Shielding Testing

Future work should also include an evaluation of the efficacy of the bonded material as applied to NTP applications. This can be accomplished both computationally and practically. Several computer programs can be used that simulate particle and radioactive decay behavior with excellent precision. Programs that would be well suited for this purpose include Geant4 and MCNP. TRIM (TRansport of Ions in Matter) code can also be used, however Geant4 and MCNP have increased capabilities for modeling a NRE. The practical sample can also be used at a research reactor to test neutron and gamma ray attenuation characteristics. The sample should be placed as a barrier between reactor and detector to understand the effects of the sample on the radiation emitting from the reactor. To provide accurate test results, the reactor material should be like the shape and content of NRE. Historically, the reactor material should have been high-enriched uranium. However, recent research has developed to use low-enriched uranium in NRE to reduce proliferation risks and costs. Therefore, more useful tests will use low-enriched uranium as reactor material to test the sample.

References

[1] Sutton, George Paul, and Oscar Biblarz. *Rocket Propulsion Elements*. Wiley, 2017.

[2] *Thermal Fluid Analysis for Nuclear Thermal Propulsion Radiation Shield*. Marshall Space Flight Center, Aug. 2015, https://tfaws.nasa.gov/wp-content/uploads/TFAWS2015-AT-04.pdf.

[3] United States, Congress, Finseth, J. L. *Rover Nuclear Rocket Engine Program: Overview of Rover Engine Tests, Final Report*, Sverdrop Corp. 1991, pp. 143-144.

[4] Emrich, William. *Principles of Nuclear Rocket Propulsion*. Elsevier Science, 2016.

[5] Heilbronn, L., "Neutron Properties and Definitions." Johnson Space Center, July, 2015.

[6] McAlister, D.R., "Gamma Ray Attenuation Properties of Common Shielding Materials." PG Research Foundation, Inc. 1955

[7] Evans, R.D., "The Atomic Nucleus". Krieger Pub Co., 1982.

[8] Olson, David L. ASM Handbook. ASM International, 1993.

[9] Mateus, L., et al. "316L Stainless Steel Diffusion Bonding Optimized Parameters." ABCM International Congress of Mechanical Engineering, December 2017.

[10] Brush Wellman Alloy Products. (2010, March). *Issue No. 15 - Grain Size and Material Strength*. Materion. Retrieved from https://materion.com/-/media/files/alloy/newsletters/technical-tidbits/issue-no-15---grain-size-and-material-strength.pdf

[11] Akselsen, O. M. "Review: Diffusion Bonding of Ceramics." Journal of Material Science, 1992.

[12] *Ceramic Materials Properties Charts*. Ceramic Industry RSS. (n.d.). Retrieved from https://www.ceramicindustry.com/ceramic-materials-properties-charts/#Boron%20Carbide

[13] *American Metal Company. (n.d.). 316L Stainless Steel Technical Data Sheet.* Retrieved from https://www.metalshims.com/t-316L-Stainless-Steel-technical-data-sheet.aspx

[14] Thyssenkrupp Materials (UK). (n.d.). *Stainless Steel 316L - 1.4404 Data Sheet*. Materials UK. Retrieved from https://www.thyssenkrupp-materials.co.uk/stainless-steel-316l-14404.html

[15] 3M Science Applied to Life. (2017). *3M advanced materials division 3M boron carbide*. Retrieved from https://multimedia.3m.com/mws/media/1004125O/3m-boron-carbide.pdf

[16] *Isabellenhütte USA. (2020, August). 1/1 Data Sheets Pure Nickel - Isabellenhuette.* Retrieved from https://www.isabellenhuette.de/fileadmin/Daten/Praezisionslegierungen/Datenblaetter_Widerstand/Englisch/PURE_NICKEL.pdf

[17] “ASTM Standard C1161-13, 2014, “Standard Test Methods for Flexural Strength of Advanced Ceramics at Ambient Temperature,” ASTM International, West Conshohocken, PA, 2014

Appendix A: Final Sample Optical Microscopy Images

Figure A.1: Composite Image at 130 Times Magnification

Figure A.2: Composite Image at 250 Times Magnification

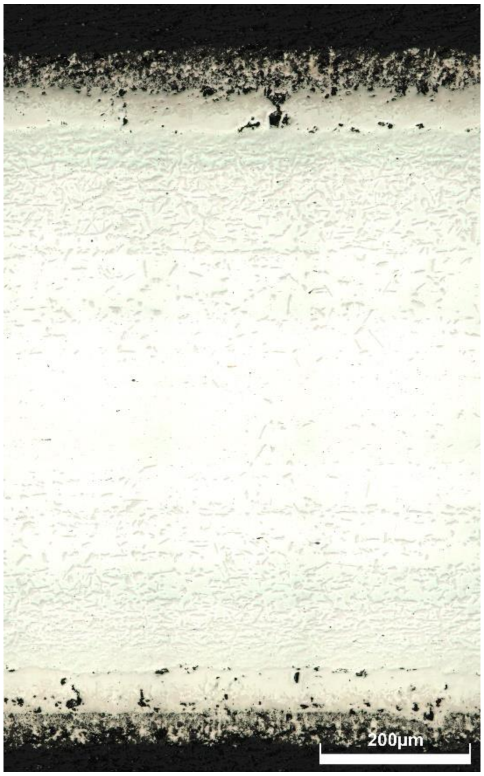

Figure A.3: Composite Image at 550 Times Magnification

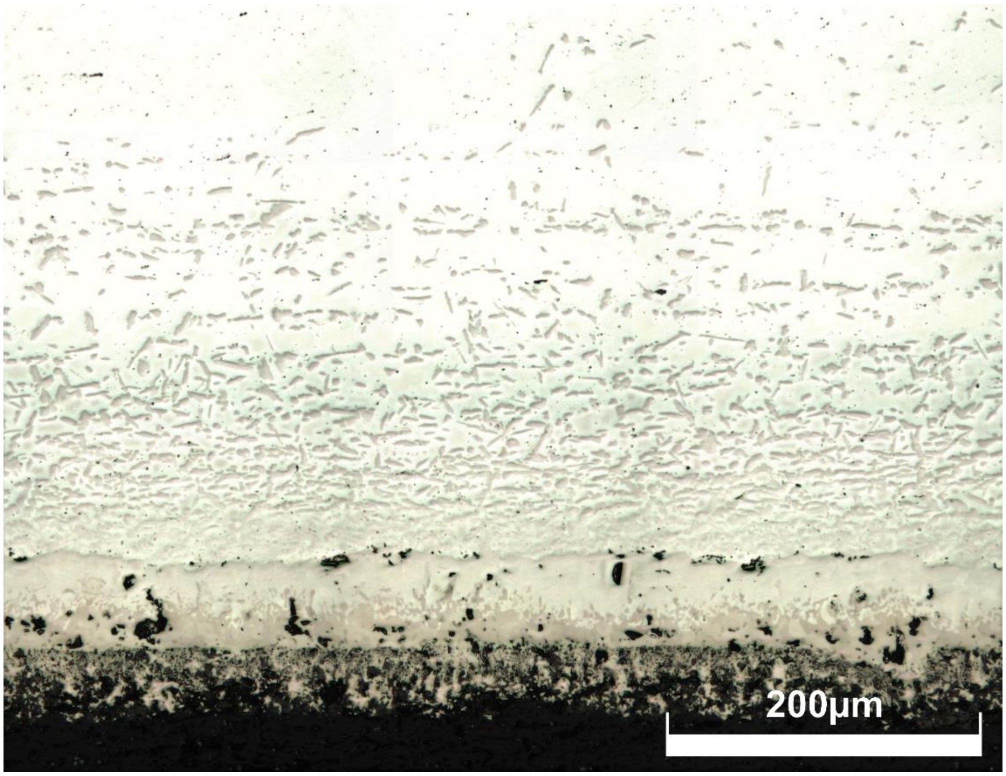

Figure A.4: Composite Image Adjusted for Clarity at 550 Times Magnification

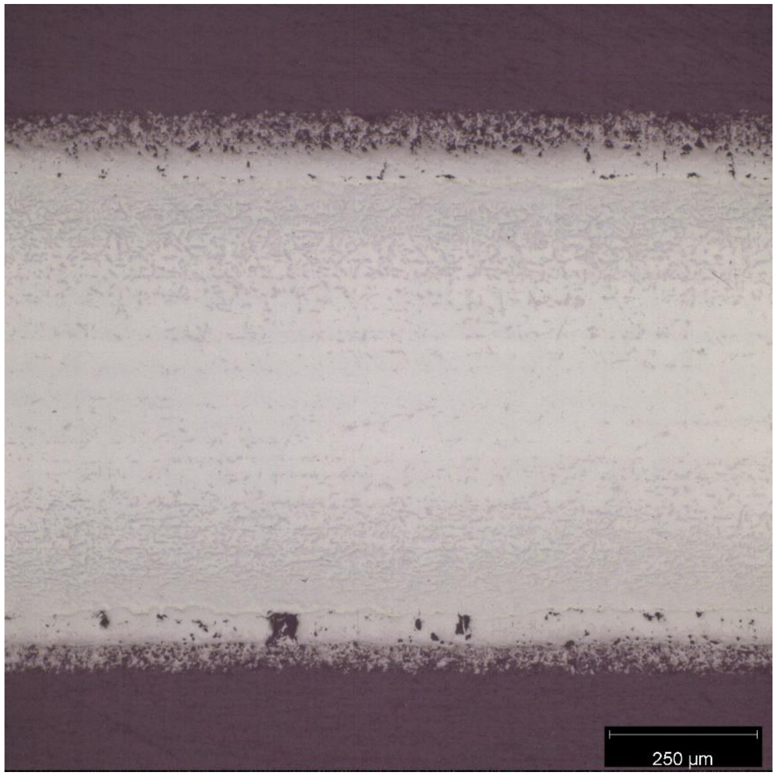

Figure A.5: Irregular B4C Distribution at 100 Times Magnification

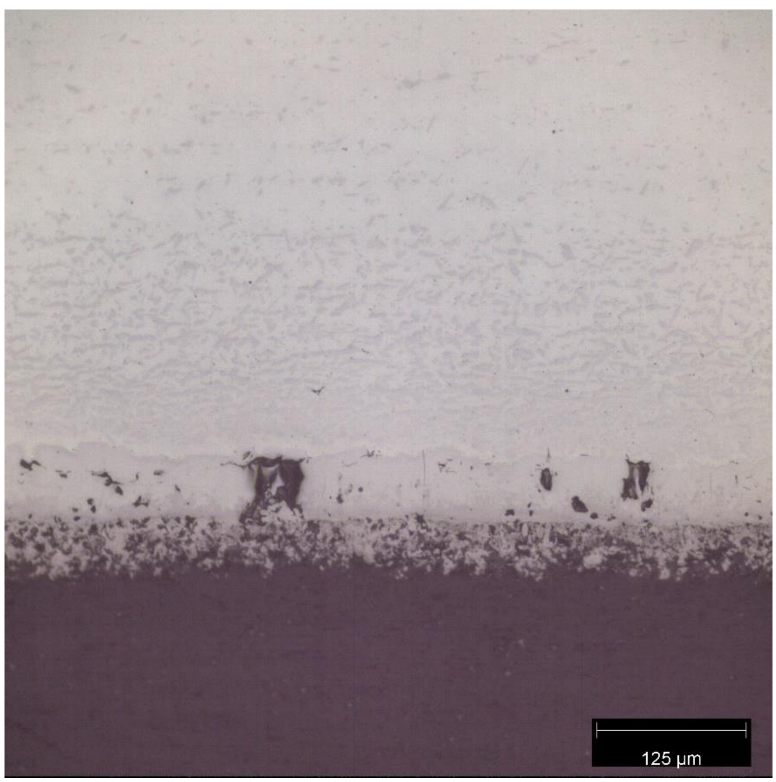

Figure A.6: Irregular B4C Distribution at 200 Times Magnification

Figure A.7: Irregular B4C Distribution at 500 Times Magnification

Figure A.8: Sample Edge at 100 Times Magnification

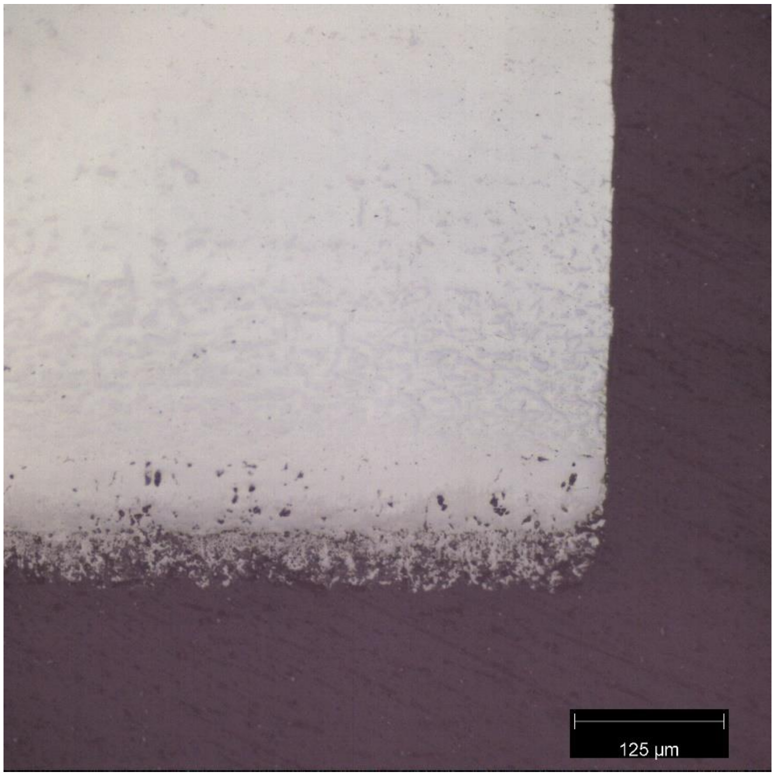

Figure A.9: Sample Edge at 200 Times Magnification

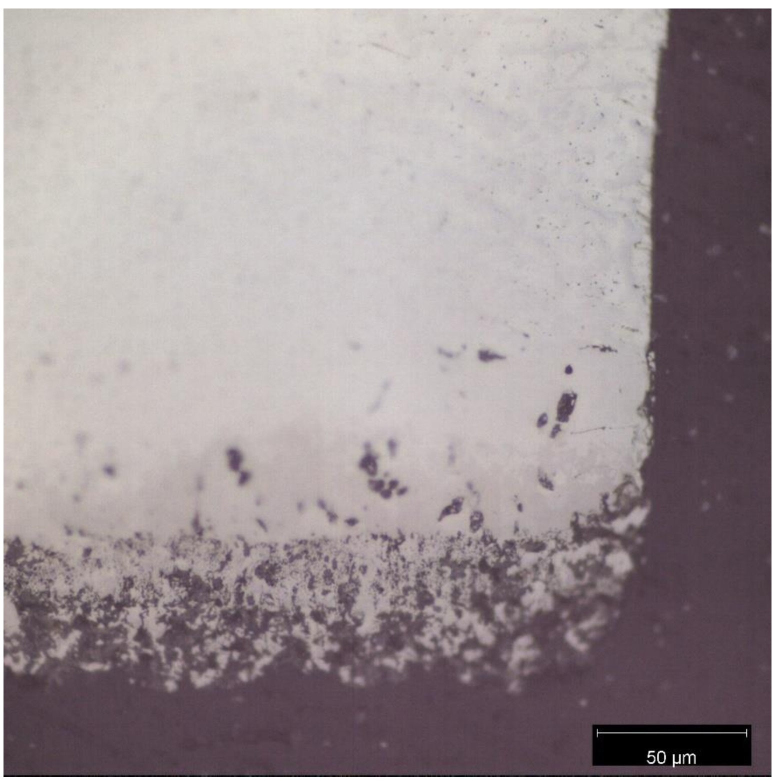

Figure A.10: Sample Edge at 500 Times Magnification

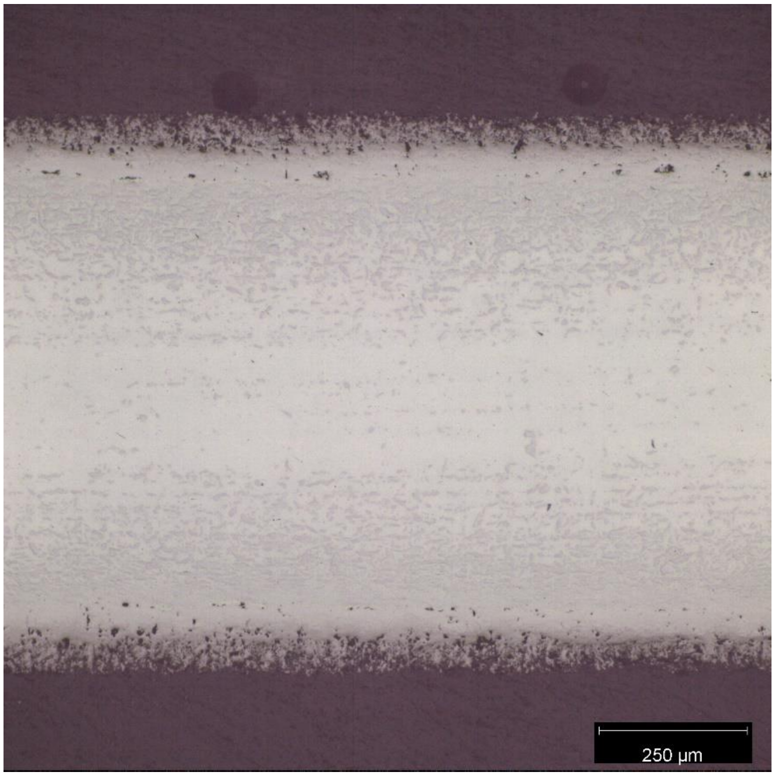

Figure A.11: Representative Bond Quality Image at 100 Times Magnification

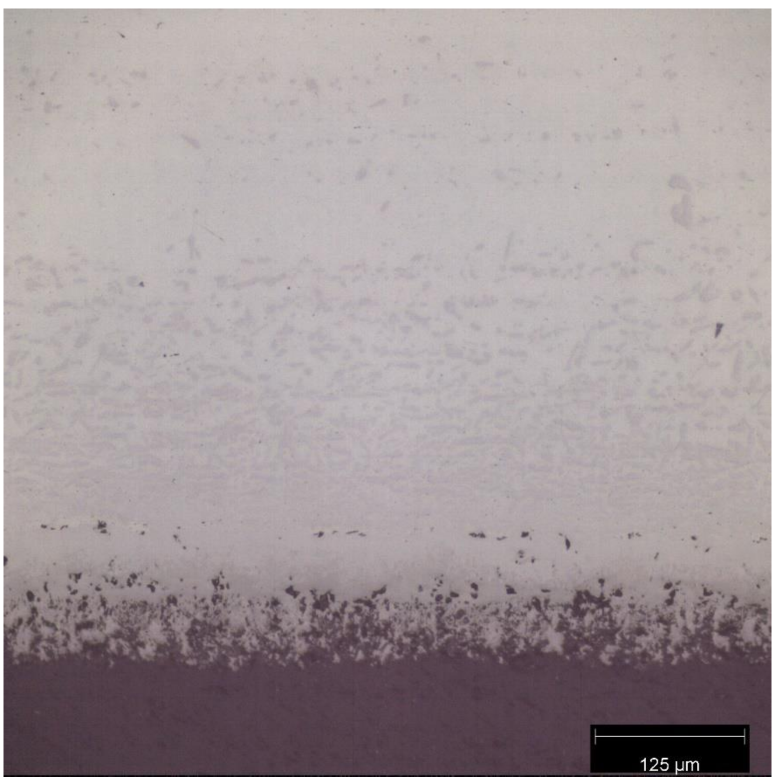

Figure A.12: Representative Bond Quality Image at 200 Times Magnification

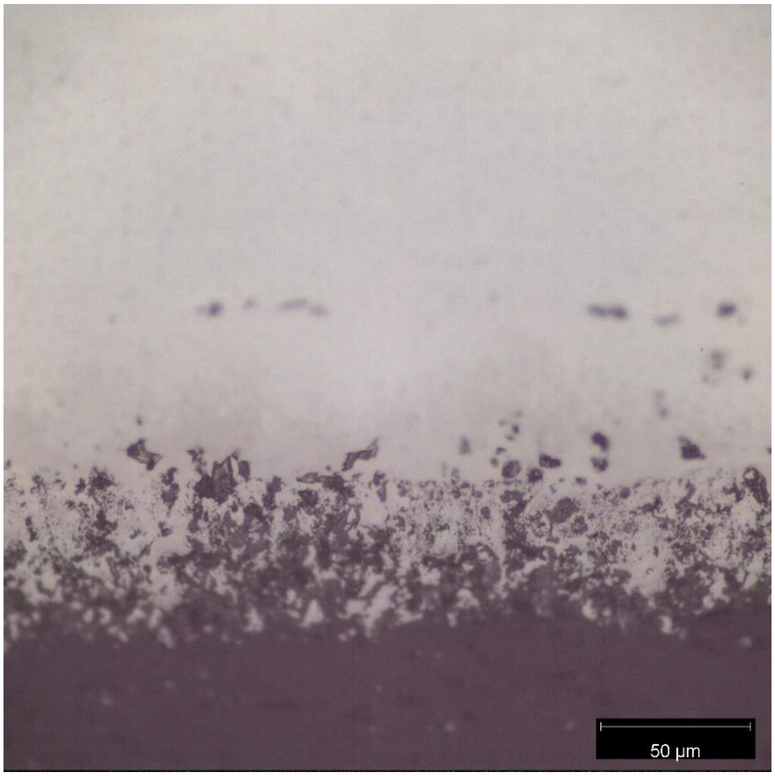

Figure A.13: Representative Bond Quality Image at 500 Times Magnification